using hydrogen peroxide as oxygen source. However, these catalytic reactions were performed in a mixture of acetonitrile and dichloromethane over a reaction time of 1 h. During the course of the present work, efficient metalloporphyrin-catalyzed H_2O_2 olefin epoxidations were reported by Montanari et al.[21b,c] for reactions run in the presence of a small amount of benzoic acid; in this case, the highest catalytic activities were observed with Mn(TDCPP)Cl as catalyst.

The absence of oxygenase activity cannot be attributed, in the present case, to the formation of a bis(imidazole) adduct with iron-porphyrin complexes, since the dismutation reaction is still catalyzed by the iron complexes in the same reaction conditions. In addition, it must be noted that the oxygenase activity is always less important with the superstructured basket-handle porphyrin complexes than with TMP or TDCPP ligands (Table II). So, a distal chain acts as a screen and enhances the steric discrimination between possible substrates for the high-valent metal-oxo intermediate complex (the approach of hydrogen peroxide, a smaller molecule than cyclohexene, to the metal-oxo species is less restricted with complexes **1-5** compared to complexes **7-10**).

Conclusion

From these studies on the catalase activity of various manganese and iron complexes, with or without a nonexchangeable axial oxygen or nitrogen ligand, the main following features can be noted: (i) the presence of free imidazole is always necessary to induce an heterolytic cleavage of H_2O_2—distal effect—and obtain efficient reactions, (ii) during competitive hydrogen peroxide dismutation and cyclohexene epoxidation reactions, the dismutation reaction is more rapid than the olefin oxygenation, (iii) all manganese porphyrins are more efficient than their iron analogues, (iv) a nitrogen base as proximal ligand favors the hydrogen peroxide dismutation compared to an oxygen atom from an alkoxo or phenoxo ligand, and (v) under our conditions, iron porphyrins have no detectable oxygenase activity.

The highest catalase activity is obtained with a synthetic system having manganese as metal and nitrogen as base, whereas the enzyme itself has iron as metal and a phenoxo from a tyrosine as axial ligand. But it is clear that the system "Mn/N-base" gives also the highest oxygenase activity, which might be destructive for the oxidizable amino acid residues of the distal side of the active site in enzyme. The iron porphyrins with an oxygen proximal ligand—especially Fe(-Ph-O-prox)(-C_{10}-), which is a true model of the catalase active site—still conserve a reasonable catalase activity and have no potentially destructive oxygenase activity at all; this could be the reason that the prosthetic group of catalase consists of an oxygen-containing ligand as a proximal ligand of a ferriprotoporphyrin IX.

Acknowledgment. We are grateful for the detailed and extensive comments of two reviewers.

Contribution from the Department of Chemistry and Biochemistry, University of Notre Dame, Notre Dame, Indiana 46556

Water-Soluble Ferric Porphyrinates: Solution and Solid-State Species

Marie A. Ivanca, A. Graham Lappin,* and W. Robert Scheidt*

Received July 3, 1990

The nature of the aqueous solution axial ligands of the water-soluble iron(III) porphyrinates $[Fe(TMPyP)]^{5+}$ and $[Fe(TPPS)]^{3-}$ has been examined as a function of pH by ^1H NMR spectroscopy. The NMR shifts provide indirect evidence for the existence of $[Fe(TPPS)(H_2O)_2]^{3-}$, $[Fe(TPPS)(H_2O)(OH)]^{4-}$, and $[(Fe(TPPS))_2O]^{8-}$ in the $[Fe(TPPS)]^{3-}$ system and $[Fe(TMPyP)(H_2O)_2]^{5+}$, $[Fe(TMPyP)(H_2O)(OH)]^{4+}$, $[(Fe(TMPyP))_2O]^{8+}$, and $[Fe(TMPyP)(OH)_2]^{3+}$ in the $[Fe(TMPyP)]^{5+}$ system. Estimates of the distribution of the species from the NMR spectra allows approximation of the various equilibrium constants in the $[Fe(TPPS)]^{3-}$ system. The pH-dependent equilibria for $[Fe(TPPS)]^{3-}$ and $[Fe(TMPyP)]^{5+}$ correspond qualitatively with previously published results. Attempts to prepare crystalline species at various pH's were successful only for the high pH form of $[Fe(TMPyP)]^{5+}$. A single-crystal structure determination shows that this species has the idealized composition $[(Fe(TMPyP))_2O](ClO_4)_8 \cdot 4H_2O$. The five-coordinate iron atom has an axial Fe-O bond distance of 1.750 (2) Å, while the average $Fe-N_p$ bond distance is 2.080 (8) Å; the iron(III) atom is 0.47 Å out of the porphyrin plane. Crystal data: a = 32.06 (2) Å, b = 18.492 (9) Å, c = 17.17 (2) Å, β = 108.6 (1)°, monoclinic, space group $C2/c$, V = 9650 (2) Å^3, Z = 4, $Fe_2Cl_8O_{37}N_{16}C_{88}H_{80}$, 5188 observed data, $R_1(F_o)$ = 0.125, $R_2(F_o)$ = 0.140, all observations at 118 K.

Water molecules and hydroxide ions are potentially important ligands for iron in hemoproteins, and protein crystal structures have shown such coordinated ligands in the ligand binding pockets of a number of heme proteins.[1-5] It would thus seem desirable to define the aqueous interaction of the iron porphyrinates over a significant pH range. The aqueous solution chemistry of naturally occurring iron porphyrinates is difficult to investigate owing to their low solubility and strong tendency to aggregate in polar solvents.[6] Synthetic ferric water-soluble porphyrins have been used to avoid the aggregation and solubility problems. Aggregation is largely avoided by use of bulky peripheral groups while water solubility is obtained through charged peripheral substituents. The two most common such synthetic derivatives are the negatively charged $[Fe(TPPS)]^{3-}$ and the positively charged $[Fe(TMPyP)]^{5+}$ species.[7]

(1) Cytochrome P-450: Poulos, T. L.; Finzel, B. C.; Howard, A. J. *Biochemistry* **1986**, *25*, 5314.
(2) Cytochrome *c* peroxidase: Finzel, B. C.; Poulos, T. L.; Kraut, J. *J. Biol. Chem.* **1984**, *259*, 13027. Poulos, T. L.; Freer, S. T.; Alden, R. A.; Edwards, S. L.; Skogland, U.; Takio, K.; Eriksson, B.; Xuong, N.; Yonetani, T.; Kraut, J. *J. Biol. Chem.* **1980**, *255*, 575.
(3) Erythrocruorin: Steigemann, W.; Weber, E. *J. Mol. Biol.* **1979**, *127*, 309.
(4) Methemoglobin: Ladner, R. C.; Heidner, E. J.; Perutz, M. F. *J. Mol. Biol.* **1977**, *114*, 385. Anderson, L. *J. Mol. Biol.* **1973**, *79*, 495.
(5) Metmyoglobin: Takano, T. *J. Mol. Biol.* **1977**, *110*, 537. Kendrew, J. C. *Science* **1963**, *139*, 1259. Kendrew, J. C.; Dickerson, R. E.; Strandberg, B. E.; Hart, R. G.; Davies, D. R.; Phillips, D. C.; Shore, V. C. *Nature* **1960**, *185*, 422.
(6) White, W. I. In *The Porphyrins*; Dolphin, D., Ed.; Academic: New York, 1978; Vol. 5, pp 303-335.
(7) Abbreviations used: H_2TPPS, tetrakis(4-sulfonatophenyl)porphyrin; H_2TMPyP, tetrakis(1-methylpyridinium-4-yl)porphyrin; H_2TAPP, tetrakis(*N*,*N*,*N*-trimethylanilinium-4-yl)porphyrin; H_2TPP, tetraphenylporphyrin; H_4FF, face-to-face porphyrin; H_2ODM, 5,15-dimethyl-2,3,7,8,12,13,17,18-octaethylporphyrin; NCH_3TPP, monoanion of *N*-methyl-*meso*-tetraphenylporphyrin; $H_2ProtoMe_2$, protoporphyrin IX dimethyl ester; H_2Porph, water-soluble porphyrin ligand; DMSO-d_6, dimethyl-d_6 sulfoxide; DSS, 2,2-dimethyl-2-silapentane-5-sulfonate; HIm, imidazole.

0020-1669/91/1330-0711$02.50/0

The pH-dependent equilibria of the $[Fe^{III}(TMPyP)]^{5+}$ [8-15] and $[Fe^{III}(TPPS)]^{3-}$ [13-20] derivatives have been previously studied by optical spectroscopy and magnetic susceptibility measurements. However, there remains some uncertainty about the coordination geometries and ligands to iron as a function of pH. There are limited ^1H NMR data for $[Fe(TPPS)]^{3-}$ and $[Fe(TMPyP)]^{5+}$ at high and low pH.[21] We have studied the ^1H NMR spectra of $[Fe(TPPS)]^{3-}$ and $[Fe(TMPyP)]^{5+}$ derivatives over the pD range 2-12. The identities of four distinct species, differing in axial ligation, have been deduced from the ^1H NMR spectra; $[Fe(Porph)(H_2O)_2]$, $[Fe(Porph)(H_2O)(OH)]$, $[Fe(Porph)(OH)_2]$, and $[Fe(Porph)]_2O$, although evidence for all species has not been found in both porphyrin systems.

We have also attempted to prepare single crystals of the various pH forms of $[Fe(TPPS)]^{3-}$ and $[Fe(TMPyP)]^{5+}$. We have obtained crystalline $[(Fe(TMPyP))_2O](ClO_4)_8$ and report its molecular structure as determined from a single-crystal X-ray study. We have also obtained a low pH derivative, crystalline $[Fe(TMPyP)(H_2O)_2](ClO_4)_5$, although the crystal structure analysis has not been completed owing to difficulties with disorder. The two crystalline complexes do suggest that certain structural problems, namely poorly defined counterions and solvent disorder, will be generally found as difficulties for these classes of porphyrin derivatives.

Experimental Section

General Information. The free base porphyrins were purchased from Midcentury (Posen, IL). Iron was inserted into H_2TPPS^{4-} as previously described.[16] The iron derivative of H_2TMPyP^{4+} was prepared as published[10] and precipitated with acetone (60% yield) instead of the published lyophilization procedure. All metalloporphyrins were characterized by their visible spectra and compared with published values.[10,16] *Caution! The perchlorate salts in the preparation are potentially explosive when heated or shocked.*[22] *Handle them in milligram quantities with care.* All reagents were used as commercially available. Dowex 50W-X8 was used for the H^+ cation exchange and Dowex 1X8-400 for the chloride ion exchange columns. D_2O (99.9%) and NaOD (99.8%) were purchased from Cambridge Isotopes and DCl (20 wt % solution in D_2O), sodium acetate-d_3 (99+% D), DMSO-d_6 (99.9%), acetic-d_3 acid-d (99.5% D), and DSS were obtained from Aldrich. The pH was measured by using a Corning Model 104 meter with an Ingold electrode specifically designed for NMR tubes. UV-vis spectra were recorded on a Perkin-Elmer Lambda 4C spectrometer, and NMR spectra were obtained by using a General Electric 300-MHz spectrometer. Graphical analysis for pH-dependent equilibria and Beer's law plots were performed by using standard least-squares procedures.

Beer's law plots for $[Fe(TPPS)]^{3-}$ and $[Fe(TMPyP)]^{5+}$ were monitored at pH = 2 over the concentration range of 1×10^{-2} to 5×10^{-6} in aqueous potassium nitrate, $\mu = 0.1$ M. Linear plots were obtained for both species. $[Fe(TPPS)]^{3-}$ obeys Beer's law within these concentrations and ionic strength at pH = 10, but $[Fe(TMPyP)]^{5+}$ deviates under the same conditions as found in similar experiments.[10]

Crystal Structure Determination of $[(Fe(TMPyP))_2O](ClO_4)_8 \cdot 4H_2O$. The crystallization procedure used the initial portion of a previously described synthesis.[10] A 10-fold excess of NaCl was added to the perchlorate salt of $[Fe(TMPyP)]^{5+}$ (~0.2 g) in 150 mL of water. Acetone was layered over this mixture (pH ~ 8) and porphyrin crystals were formed (~20 days) with cocrystallization of NaCl and evaporation of layered acetone and water. The crystals contain only perchlorate as the counterion; a qualitative test for chloride ion was negative.

Table I. Crystallographic Data for $[(Fe(TMPyP))_2O](ClO_4)_8 \cdot 4H_2O$

$Fe_2Cl_8O_{37}N_{16}C_{88}H_{80}$	fw = 2335.0
a = 32.06 (2) Å	space group: $C2/c$
b = 18.492 (9) Å	T = 118 K
c = 17.17 (2) Å	$\bar{\lambda}$ = 0.71073 Å
β = 108.6 (1)°	μ = 0.612 mm^{-1}
V = 9650 (2) Å^3	$R_1(F_o)$ = 0.125
Z = 4	$R_2(F_o)$ = 0.140

Preliminary X-ray data, at room temperature, showed that a low-temperature data set with a freshly prepared crystal would be required. The low-temperature data set was collected with a dark brown crystal (0.30 × 0.15 × 0.35 mm) to a maximum 2θ = 54.90° on an Enraf-Nonius CAD4 diffractometer utilizing graphite-monochromated Mo Kα radiation. The crystal has a four-molecule, monoclinic unit cell with final cell constants reported in Table I. Complete crystallographic details including all data collection parameters are given in supplementary Table SI. Data reduction using the Blessing suite of programs[23] gave 5188 observed reflections.

The direct methods programs MULTAN and DIRDIF[24] served to locate the iron and oxo atoms, all atoms of the porphyrin core and one *N*-methylpyridinium-4-yl ring. A series of difference Fourier calculations located most remaining atoms. However, the maps showed the anions and solvate molecules as diffuse peaks and also suggested disorder problems involving two of the perchlorate anions, the water molecules and one peripheral *N*-methylpyridinium-4-yl ring. This ring had two distinct orientations with similar occupancy factors and was described by two rigid groups with ring geometry obtained from the structural data of $[Ni(TMPyP)(HIm)_2](ClO_4)_4$.[25] Rigid-group, least-squares refinement gave final ring occupancies of 0.54 and 0.46. The ring positions appeared correlated with a perchlorate ion that was also disordered over two distinct positions separated by 3.27 Å. Additionally, water molecules are located in the region and appear to alternatively occupy space when the perchlorate ion is in the alternate location. With equivalent occupancies for the *N*-methylpyridiniumyl ring and the perchlorate ion, all nonbonded contacts have reasonable values. The other disordered perchlorate shows two distinct orientations with the chlorines separated by 0.48 Å. The two perchlorate orientations were refined as rigid groups with Cl-O distances of 1.42 Å.[26] Final refined occupancy factors are 0.73 and 0.27. Four distinct, partial occupancy water molecule sites were found; three are hydrogen bonded to the disordered perchlorate ions.

Least-squares refinement was then carried to convergence with anisotropic temperature factors for all ordered atoms with the exception of one oxygen of one of the ordered perchlorates; isotropic temperature factors were given to the disordered groups with the exception of one water and one perchlorate ion. The final difference Fourier calculation showed no significant features; the largest peak had a peak height of 0.42 e/Å^3 near one of the α-carbons of the porphinato core. At convergence, the final value of the unweighted R was 0.125 and the weighted R was 0.140. Final values of atomic coordinates are reported in Table II and final values of the anisotropic temperature factors are in Table SII. Rigid group parameters and derived atomic coordinates of one *N*-methylpyridinium-4-yl ring and one perchlorate anion are given in Tables SIII and SIV.

A number of attempts were made to obtain crystalline $[Fe(TMPyP)]^{5+}$ and $[Fe(TPPS)]^{3-}$ derivatives under low pH conditions. The one successful crystallization procedure unfortunately yields an im-

(8) Miskelly, G. M.; Webley, W. S.; Clark, C. R.; Buckingham, D. A. *Inorg. Chem.* **1988**, *27*, 3773.
(9) Tondreau, G. A.; Wilkins, R. A. *Inorg. Chem.* **1986**, *25*, 2745.
(10) Pasternack, R. F.; Lee, H.; Malek, P.; Spencer, C. *J. Inorg. Nucl. Chem.* **1977**, *39*, 1865.
(11) Kurihara, H.; Arifuku, F.; Ando, I.; Saita, M.; Nishino, R.; Ujimoto, K. *Bull. Chem. Soc. Jpn.* **1982**, *55*, 3515.
(12) Kobayashi, N.; Koshiyama, M.; Osa, T.; Kuwana, T. *Inorg. Chem.* **1983**, *22*, 3608.
(13) Goff, H.; Morgan, L. O. *Inorg. Chem.* **1976**, *15*, 3180.
(14) McLendon, G.; Bailey, M. *Inorg. Chem.* **1979**, *18*, 2120.
(15) Harris, F. L.; Toppen, D. L. *Inorg. Chem.* **1978**, *17*, 71.
(16) Fleischer, E. B.; Palmer, J. M.; Srivastava, T. S.; Chatterjee, A. *J. Am. Chem. Soc.* **1971**, *93*, 3162.
(17) Sutter, J. R.; Hambright, P.; Chock, P. B.; Krishnamurthy, M. *Inorg. Chem.* **1974**, *13*, 2764.
(18) Taniguchi, V. T. Ph.D. Thesis, University of California, Irvine, 1978.
(19) El-Awady, A. A.; Wilkins, P. C.; Wilkins, R. A. *Inorg. Chem.* **1985**, *24*, 2053.
(20) Barley, M. H.; Takeuchi, K. J.; Meyer, T. J. *J. Am. Chem. Soc.* **1986**, *108*, 5876.
(21) Goff, H. M.; Morgan, L. O. *Bioinorg. Chem.* **1978**, *9*, 61.
(22) Wolsey, W. C. *J. Chem. Educ.* **1973**, *50*, A335. *Chem. Eng. News* **1983**, *61* (Dec. 5), 4; **1963**, *41* (July 8), 47.
(23) Blessing, R. H. *Crystallogr. Rev.* **1987**, *1*, 3.
(24) Programs used in this study include Beurskens, Bosman, Doeburg, Gould, van der Hark, Prick, Noordik, Stempel and Smits' DIRDIF, local modifications of Main, Hull, Lessinger, Germain, Declerq, and Woolfson's MULTAN, Jacobson's ALLS, Zalkin's FORDAP, Busing and Levy's ORFFE and ORFLS, and Johnson's ORTEP2. Atomic form factors were taken from: Cromer, D. T.; Mann, J. B. *Acta Crystallogr., Sect. A* **1968**, *A24*, 321. Real and imaginary corrections for anomalous dispersion in the form factor of the iron and chlorine atoms were taken from: Cromer, D. T.; Lieberman, D. J. *J. Chem. Phys.* **1970**, *53*, 1891. Scattering factors for hydrogen were taken from: Stewart, R. F.; Davidson, E. R.; Simpson, W. T. *J. Chem. Phys.* **1965**, *42*, 3175. All calculations were performed on VAX 11/730 or 3200 computers.
(25) Kirner, J. F.; Garofalo, J., Jr.; Scheidt, W. R. *Inorg. Nucl. Chem. Lett.* **1975**, *11*, 107.
(26) Schilt, A. A. *Perchloric Acid and Perchlorates*; The G. Frederick Smith Chemical Co.: Columbus, OH, 1979; p 4.

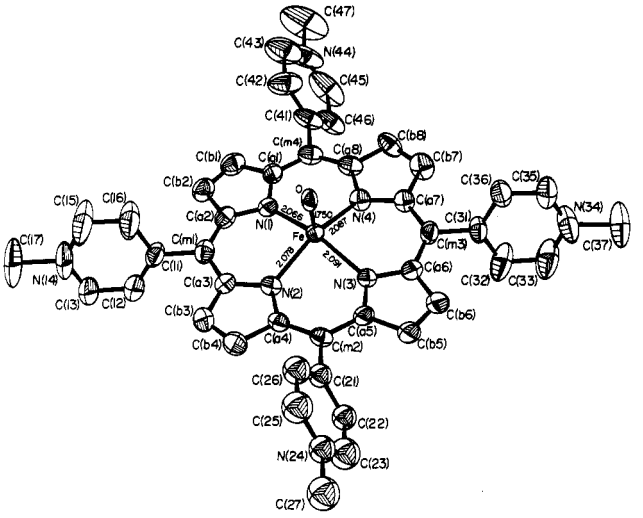

Figure 1. ORTEP2 drawing of the crystallographically unique half of the μ-oxo complex $[(Fe(TMPyP))_2O](ClO_4)_8 \cdot 4H_2O$ (50% probability surfaces). Coordination group distances and atomic labels are shown.

pure material.[27] The procedure used three separate solutions carefully layered in an 18 × 150 mm test tube. A saturated sodium perchlorate and HCl–KCl solution[28] (HCl–KCl, pH 1.0) was separated from top layer (6×10^{-3} M of the $[Fe(TMPyP)]^{5+}$ chloride salt in HCl–KCl) by the pure HCl–KCl solution (2:1:2). Brown needle crystals (as long as 25 mm) formed. Many other crystallization attempts (with no added chloride ion) were unsuccessful.

NMR Experiments. pH-dependent NMR spectra for $[Fe(TPPS)]^{3-}$ and $[Fe(TMPyP)]^{5+}$ were collected between pD 2.2 and 12.3 in increments of 1 pD unit and smaller where changes in spectra occurred. All spectra were recorded at 22 °C, and in general, 1800 acquisitions were obtained over a spectral width of 18 kHz for $[Fe(TPPS)]^{3-}$ and 28 kHz for $[Fe(TMPyP)]^{5+}$. Delay times between acquisitions were chosen to be $\geq 5T_2$ for the slowest relaxing species throughout the pH range. A saturated solution of DSS in D_2O was used as an external reference for all samples.[29] The sodium salt of $[Fe(TPPS)]^{3-}$ or the chloride salt of $[Fe(TMPyP)]^{5+}$ was dissolved in D_2O ($\sim 6.0 \times 10^{-3}$ M); individual samples were prepared at each pH value. The NMR spectra were measured at an ionic strength of 0.1 M in KNO_3 media. Measurements were also made on solutions with ionic strengths of 0.2 M (KNO_3 and phosphate buffer) and 0.1 M (acetate buffer) and with no added electrolyte. DCl and NaOD were used to adjust the pH*,[30,31] which was measured before and after each NMR spectrum. All solutions reached apparent equilibrium before the NMR experiments began.[32] The UV–vis spectrum of each solution was checked after each NMR run. In the $[Fe(TMPyP)]^{5+}$ system, this indicated the presence of a slight precipitate at a very high pH.

Results

Structure of $[(Fe(TMPyP))_2O](ClO_4)_8 \cdot 4H_2O$. Structural analysis of the crystalline complex obtained at high pH ($\sim$8.5) shows it is a μ-oxo complex with idealized formula $[(Fe(TMPyP))_2O](ClO_4)_8 \cdot 4H_2O$. The μ-oxo complex has a crystallographically required 2-fold axis of symmetry through the oxo ligand; the crystallographically unique half of the molecule is illustrated in Figure 1. The Fe–O–Fe angle is 175.1 (7)°. The

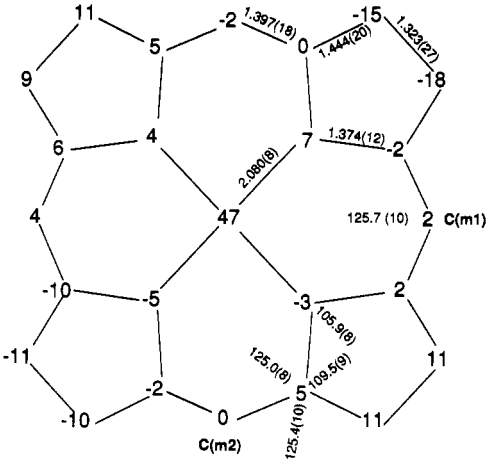

Figure 2. Formal diagram of the porphinato core in $[(Fe(TMPyP))_2O]^{8+}$ showing the averaged values of bond distances and angles in the 24-atom porphinato core. Values of the perpendicular displacement, in units of 0.01 Å, of each atom from the 24-atom mean plane are shown.

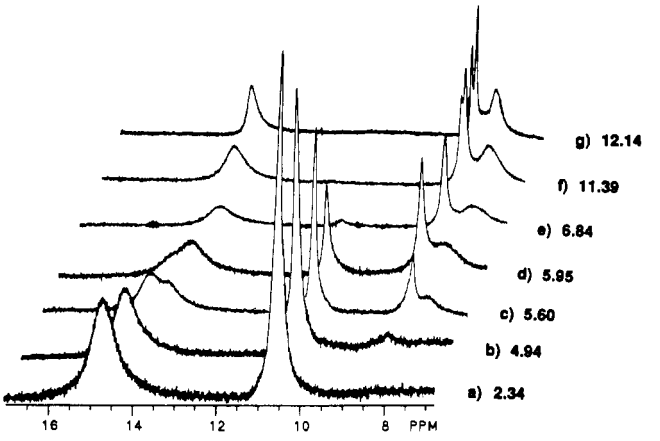

Figure 3. Proton NMR spectra for the $[Fe(TPPS)]^{3-}$ system between 6.8 and 17.0 ppm at 298 K and pH between 2.34 and 12.14. Each stacked spectrum is offset from the one below by 0.5 ppm.

average separation between the two porphinato cores of the μ-oxo dimer is 4.43 Å. The average iron–nitrogen distance is 2.081 (8) Å and the iron–oxygen distance is 1.750 (2) Å. The iron(III) atom is 0.47 Å out of the mean porphyrin plane. The N–Fe–Fe–N dihedral angle is 32.4 (3)°. Selected values of bond distances and bond angles for the $[(Fe(TMPyP))_2O](ClO_4)_8 \cdot 4H_2O$ molecule are recorded in Table III; a complete set is given in Table SVI.

Figure 2 shows the displacement of each atom from the mean plane of the porphinato core. The crystallographically unique porphyrin ring has a saddle-shaped conformation (Figure 2). This structural feature along with relatively small values for the dihedral angles of the *N*-methylpyridinium-4-yl ring with the mean plane of the core suggest[33,34] an intermolecular π–π interaction between porphinato cores. Indeed, an examination of the crystal structure shows a porphyrin ring to porphyrin ring interaction between two binuclear $[(Fe(TMPyP))_2O]^{8+}$ units. The intermolecular center–center distance is 6.52 Å, and the Fe···Fe separation is 7.056 (3) Å; the average mean plane separation between adjacent molecules is 3.59 Å. The slip angle (center–center) is 56.6°, and the lateral shift is 5.44 Å. These values correspond with those previously found for solid-state aggregates.[34]

Four water molecule sites (all partially occupied) were found. Water molecules at two of these sites, with total occupancy of 0.56, collectively alternate occupancy with the disordered per-

(27) An X-ray crystal structure determination shows that this material is a mixture of five- (chloroiron) and six-coordinate (diaquoiron) species. The chloroiron contaminant is attributed to the high chloride ion concentration used for the crystallization medium (much higher than that in the NMR experiments).

(28) *CRC Handbook of Chemistry and Physics*; CRC: Boca Raton, FL 1983, p D-150.

(29) Corsini, A.; Herrmann, O. *Talanta* **1986**, *33*, 335.

(30) pH* in the solutions containing deuterium ions in D_2O were recorded with a pH electrode. Corrections were made for this difference where pD = 0.4 + pH*. The pH, pD, pK^H, and pK^D measurements with our electrode correspond with those in Glasoe et al.[31]

(31) Glasoe, P. K.; Long, F. A. *J. Phys. Chem.* **1960**, *64*, 188.

(32) This was checked by ensuring that each individual NMR spectrum was time invariant. In addition, the same NMR spectrum can be obtained from the acidification of the μ-oxo complex or from the diaquo complex by addition of base.

(33) Dihedral angles of the *N*-methylpyridinium-4-yl rings relative to the mean plane of the 24-atom porphinato core are 56.94, 64.79, 46.40, 60,76, and 66.25°. Five values are listed due to one disordered ring.

(34) Scheidt, W. R.; Lee, Y. J. *Structure and Bonding*; Springer-Verlag: Berlin, 1987; Vol. 64, pp 24–40, 45–54.

Table II. Fractional Coordinates of $[(Fe(TMPyP))_2O](ClO_4)_8 \cdot 4H_2O$

atom	*x*	*y*	*z*
Fe	0.02258 (5)	0.11810 (7)	0.66978 (9)
Cl(1)	−0.1268 (4)	0.4906 (5)	0.4438 (5)
Cl(3)	0.26063 (15)	0.3785 (3)	0.91412 (24)
Cl(4)	0.0556 (4)	−0.3004 (6)	0.7442 (8)
Cl(4′)	0.1560 (4)	−0.2587 (7)	0.8571 (7)
O	0.0000	0.1141 (5)	0.7500
O(11)	−0.0958 (9)	0.5529 (16)	0.4255 (17)
O(12)	−0.1204 (12)	0.4376 (12)	0.4001 (16)
O(13)	−0.1110 (10)	0.4715 (14)	0.5191 (12)
O(14)	−0.1655 (9)	0.5088 (20)	0.4181 (22)
O(31)	0.2871 (5)	0.3498 (11)	0.9870 (8)
O(32)	0.2409 (7)	0.3350 (11)	0.8534 (14)
O(33)	0.2841 (6)	0.4223 (13)	0.8895 (12)
O(34)	0.2267 (5)	0.4183 (12)	0.9317 (10)
O(41)	0.0520 (10)	−0.3765 (12)	0.757 (3)
O(42)	0.0316 (8)	−0.3126 (17)	0.6528 (15)
O(43)	0.1037 (8)	−0.2696 (13)	0.7644 (14)
O(44)	0.0262 (9)	−0.2530 (17)	0.7835 (16)
O(41′)	0.1959 (9)	−0.2554 (15)	0.8457 (17)
O(42′)	0.1544 (13)	−0.1928 (22)	0.9032 (24)
O(43′)	0.1438 (15)	−0.3288 (26)	0.8890 (28)
O(44′)	0.1365 (20)	−0.2384 (33)	0.7834 (38)
OS′	0.0086 (16)	−0.4762 (24)	0.7110 (27)
OS1′	0.0040 (14)	−0.4459 (18)	0.6049 (24)
OS	0.1873 (15)	−0.2330 (24)	0.8218 (27)
OS1	0.2054 (23)	−0.2779 (39)	0.8561 (43)
N(1)	0.01014 (29)	0.2237 (4)	0.6296 (5)
N(2)	−0.03127 (28)	0.0879 (4)	0.5705 (5)
N(3)	0.04662 (27)	0.0133 (5)	0.6671 (5)
N(4)	0.08786 (29)	0.1496 (5)	0.7252 (6)
N(14)	−0.1850 (4)	0.3074 (9)	0.4044 (10)
N(34)	0.2336 (4)	−0.0851 (9)	0.9039 (8)
N(44)	0.1408 (8)	0.4806 (9)	0.7911 (10)
C(a1)	0.0362 (4)	0.2838 (6)	0.6585 (7)
C(a2)	−0.0276 (4)	0.2497 (6)	0.5765 (7)
C(a3)	−0.0660 (4)	0.1319 (5)	0.5301 (7)
C(a4)	−0.0472 (3)	0.0180 (6)	0.5555 (6)
C(a5)	0.0210 (4)	−0.0464 (6)	0.6368 (7)
C(a6)	0.0864 (4)	−0.0131 (6)	0.7144 (7)
C(a7)	0.1212 (3)	0.1046 (6)	0.7687 (7)
C(a8)	0.1024 (4)	0.2200 (6)	0.7448 (7)
C(b1)	0.0136 (5)	0.3475 (6)	0.6206 (8)
C(b2)	−0.0252 (5)	0.3291 (6)	0.5699 (8)
C(b3)	−0.1037 (4)	0.0878 (7)	0.4878 (8)
C(b4)	−0.0926 (4)	0.0208 (7)	0.5020 (8)
C(b5)	0.0465 (5)	−0.1108 (7)	0.6633 (8)
C(b6)	0.0865 (5)	−0.0896 (7)	0.7134 (8)
C(b7)	0.1575 (4)	0.1479 (8)	0.8166 (9)
C(b8)	0.1466 (4)	0.2174 (7)	0.8045 (8)
C(m1)	−0.0642 (4)	0.2072 (6)	0.5318 (7)
C(m2)	−0.0235 (4)	−0.0442 (6)	0.5844 (6)
C(m3)	0.1216 (4)	0.0293 (6)	0.7637 (7)
C(m4)	0.0784 (4)	0.2810 (6)	0.7132 (7)
C(11)	−0.1057 (4)	0.2457 (7)	0.4845 (8)
C(12)	−0.1231 (5)	0.2439 (8)	0.4016 (9)
C(13)	−0.1628 (5)	0.2759 (9)	0.3612 (9)
C(15)	−0.1670 (7)	0.3201 (13)	0.4860 (13)
C(16)	−0.1278 (5)	0.2855 (12)	0.5275 (10)
C(17)	−0.2299 (7)	0.3436 (12)	0.3614 (15)
C(31)	0.1622 (4)	−0.0097 (7)	0.8119 (7)
C(32)	0.1865 (5)	−0.0492 (9)	0.7723 (11)
C(33)	0.2221 (6)	−0.0893 (10)	0.8212 (12)
C(35)	0.2126 (5)	−0.0466 (8)	0.9393 (10)
C(36)	0.1776 (4)	−0.0069 (7)	0.8966 (8)
C(37)	0.2709 (5)	−0.1355 (11)	0.9532 (12)
C(41)	0.1014 (5)	0.3534 (7)	0.7404 (8)
C(42)	0.1412 (5)	0.3658 (7)	0.7279 (8)
C(43)	0.1622 (7)	0.4344 (12)	0.7538 (12)
C(45)	0.1034 (8)	0.4673 (10)	0.8058 (12)
C(46)	0.0835 (6)	0.4025 (7)	0.7791 (10)
C(47)	0.1662 (9)	0.5525 (10)	0.8193 (14)

[a] The estimated standard deviations of the least significant digits are given in parentheses.

chlorate ion whose chlorine positions are separated by 3.27 Å. Although such "dual" use of space is relatively uncommon in small molecular crystal structures, it is a frequent phenomenon in protein crystal structures.[35] A third water molecule is hydrogen bonded to this perchlorate ion; the fourth water site is occupied only when this perchlorate ion is in its alternative location.

The dihedral angle between the two planes of the disordered *N*-methylpyridinium-4-yl ring is 72.9°. Although disordered peripheral aryl groups in tetraarylporphyrin complexes is un-

Table III. Selected Bond Lengths and Angles in $[(Fe(TMPyP))_2O](ClO_4)_8 \cdot 4H_2O$[a]

A. Bond Lengths (Å)

Fe–N(1)	2.066 (8)	C(a3)–C(b3)	1.446 (16)
Fe–N(2)	2.078 (8)	C(a3)–C(m1)	1.394 (15)
Fe–N(3)	2.091 (8)	C(a4)–C(b4)	1.454 (15)
Fe–N(4)	2.087 (9)	C(a4)–C(m2)	1.380 (15)
Fe–O	1.750 (2)	C(a5)–C(b5)	1.433 (16)
N(1)–C(a1)	1.383 (13)	C(a5)–C(m2)	1.425 (16)
N(1)–C(a2)	1.351 (14)	C(a6)–C(b6)	1.415 (16)
N(2)–C(a3)	1.374 (13)	C(a6)–C(m3)	1.411 (16)
N(2)–C(a4)	1.384 (13)	C(a7)–C(b7)	1.437 (16)
N(3)–C(a5)	1.375 (13)	C(a7)–C(m3)	1.395 (15)
N(3)–C(a6)	1.366 (13)	C(a8)–C(b8)	1.462 (16)
N(4)–C(a7)	1.372 (14)	C(a8)–C(m4)	1.376 (16)
N(4)–C(a8)	1.387 (14)	C(b1)–C(b2)	1.316 (18)
C(a1)–C(b1)	1.427 (16)	C(b3)–C(b4)	1.290 (17)
C(a1)–C(m4)	1.380 (16)	C(b5)–C(b6)	1.356 (18)
C(a2)–C(b2)	1.478 (15)	C(b7)–C(b8)	1.331 (19)
C(a2)–C(m1)	1.416 (16)		

B. Bond Angles (deg)

N(1)FeN(2)	87.6 (3)	C(b3)C(a3)C(m1)	126.6 (10)
N(1)FeN(3)	154.3 (3)	N(2)C(a3)C(m1)	124.0 (10)
N(1)FeN(4)	87.0 (4)	N(2)C(a4)C(b4)	108.7 (10)
N(1)FeO	102.6 (4)	C(b4)C(a4)C(m2)	125.6 (10)
N(2)FeN(3)	87.1 (3)	N(2)C(a4)C(m2)	125.7 (10)
N(2)FeN(4)	154.0 (4)	N(3)C(a5)C(b5)	109.6 (10)
N(2)FeO	101.0 (3)	C(b5)C(a5)C(m2)	125.4 (10)
N(3)FeN(4)	86.9 (3)	N(3)C(a5)C(m2)	124.9 (10)
N(3)FeO	103.0 (4)	N(3)C(a6)C(b6)	110.8 (10)
FeOFe	175.1 (7)	C(b6)C(a6)C(m3)	124.0 (11)
FeN(1)C(a1)	127.6 (7)	N(3)C(a6)C(m3)	125.0 (10)
FeN(1)C(a2)	126.7 (7)	N(4)C(a7)C(b7)	108.7 (10)
C(a1)N(1)C(a2)	105.3 (9)	C(b7)C(a7)C(m3)	124.8 (11)
FeN(2)C(a3)	125.6 (7)	N(4)C(a7)C(m3)	126.4 (10)
FeN(2)C(a4)	124.4 (7)	N(4)C(a8)C(b8)	108.4 (11)
C(a3)N(2)C(a4)	105.5 (8)	C(b8)C(a8)C(m4)	126.7 (11)
FeN(3)C(a5)	124.9 (7)	N(4)C(a8)C(m4)	124.9 (10)
FeN(3)C(a6)	126.8 (7)	C(a1)C(b1)C(b2)	108.9 (11)
C(a5)N(3)C(a6)	105.6 (9)	C(a2)C(b2)C(b1)	105.5 (11)
FeN(4)C(a7)	124.9 (7)	C(a3)C(b3)C(b4)	108.2 (10)
FeN(4)C(a8)	125.6 (8)	C(a4)C(b4)C(b3)	108.2 (11)
C(a7)N(4)C(a8)	107.2 (9)	C(a5)C(b5)C(b6)	106.9 (11)
N(1)C(a1)C(b1)	109.9 (10)	C(a6)C(b6)C(b5)	106.9 (12)
C(b1)C(a1)C(m4)	125.8 (11)	C(a7)C(b7)C(b8)	109.0 (12)
N(1)C(a1)C(m4)	124.2 (10)	C(a8)C(b8)C(b7)	106.8 (11)
N(1)C(a2)C(b2)	110.4 (10)	C(a2)C(m1)C(a3)	125.9 (10)
N(1)C(a2)C(m1)	125.3 (10)	C(a4)C(m2)C(a5)	125.2 (10)
C(b2)C(a2)C(m2)	124.3 (11)	C(a6)C(m3)C(a7)	124.8 (10)
N(2)C(a3)C(b3)	109.4 (9)	C(a8)C(m4)C(a1)	127.0 (10)

[a] The estimated standard deviations of the least significant digits are given in parentheses.

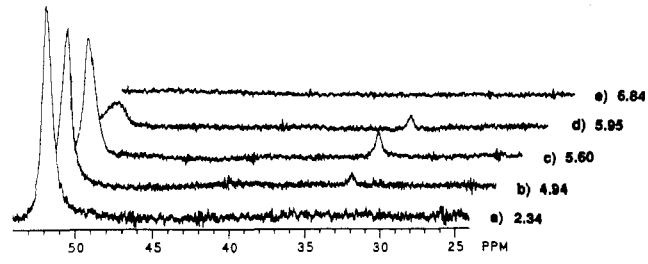

Figure 4. Proton NMR spectra for the $[Fe(TPPS)]^{3-}$ system between 24 and 54 ppm at 298 K and pH between 2.34 and 6.84. Each stacked spectrum is offset from the one below by 1.8 ppm.

(35) Finzel, B. Personal communication.

Table IV. Comparison of Selected Structural Features for (μ-Oxo)iron(III) Porphyrinate Complexes

compound	Fe–N_p[a]	Fe–O[a]	Fe–O–Fe[b]	Fe···Ct[a,c]	mean plane separation[d]	interplanar angle[b,e]	twist[b,f]	ref
$[Fe(ODM)_2]O$	2.065 (4)	1.752 (1)	178.5 (6)	0.53	4.55	2.9	3	41
$[Fe(TPP)]_2O$	2.087 (3)	1.763 (1)	174.5 (1)	0.54	4.50	3.7	35	42, 43
$[Fe(ProtoMe_2)]_2O$	2.08	1.73	172.5	0.42	4.40	5.4	28	44
$[Fe(TMPyP)]_2O$	2.080 (8)	1.750 (2)	175.1 (7)	0.47	4.43	0.4	32	this work
$[Fe(FF)]_2O{\cdot}H_2O$	2.075 (19)	1.787 (17)	161.1 (4)	0.60, 0.65	*g*	15.8	24	39
$[Fe(NCH_3TPP)(TPP)]O$	2.066 (6)	1.740 (4)	165.4 (3)	0.43 (2)		7.3	30	45

[a] Values in Å. [b] Values in degrees. [c] Fe···Ct is the iron atom displacement from the 24-atom mean plane. [d] Intramolecular separation between 24-atom cores. [e] Angle between the two 24-atom mean planes. [f] N–Fe–Fe–N dihedral angle. [g] Not applicable.

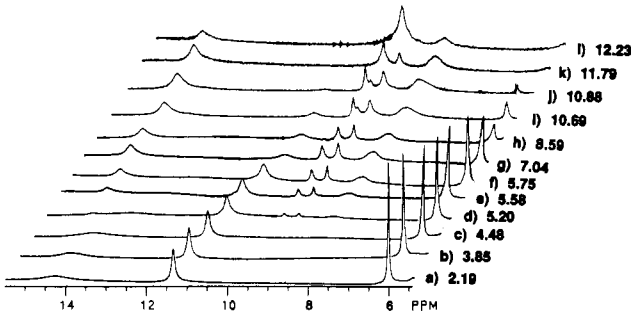

Figure 5. Proton NMR spectra of $[Fe(TMPyP)]^{5+}$ between 5.4 and 15.5 ppm at 298 K and pH between 2.19 and 12.23. Each stacked spectrum is offset from the one below by 0.3 ppm.

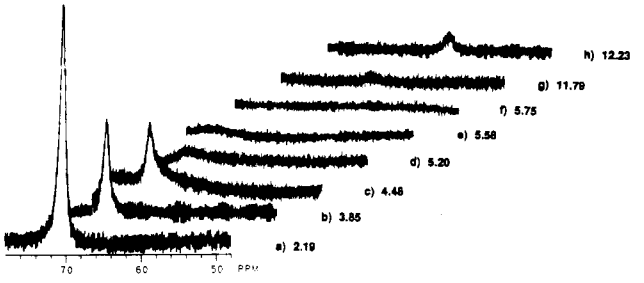

Figure 6. NMR spectra of $[Fe(TMPyP)]^{5+}$ between 48 and 78 ppm at 298 K and pH between 2.19 and 12.23. Each stacked spectrum is offset from the one below by 6.0 ppm.

common, it has been observed previously.[36]

$[Fe(TPPS)]^{3-}$ NMR. The NMR spectra of $[Fe(TPPS)]^{3-}$ between pD = 2.3 and pD = 12.2 are illustrated in Figures 3 (6.8–17.0 ppm) and 4 (24.0–54.0 ppm). Figures 3a and 4a (pD 2.34) show the limiting spectrum for $[Fe(TPPS)(H_2O)_2]^{3-}$ (proton frequencies (ppm): pyrrole β, 52.4; ortho, 14.6; meta, 10.6). The intensities of these signals decrease but are unshifted as the pD is increased to 5.95 (Figures 3b–d and 4b–d), and at higher pD (>6.84), the signals completely disappear (Figures 3e and 4e). Over the same pD range, a signal at 33.4 ppm appears (Figure 4b). This is assigned to the pyrrole β-protons of $[Fe(TPPS)(H_2O)(OH)]^{4-}$; the ortho and meta protons for this species were not observed and apparently overlap those of $[Fe(TPPS)(H_2O)_2]^{3-}$. The pyrrole β signal for the aquo/hydroxo species increases in intensity with an increase in pD from 4.94 to 5.60 (Figure 4b,c), but on a further increase in pD (>5.55) the intensity begins to decrease (Figure 4d) until the signal has completely disappeared at pD = 6.84 (Figure 4e). In turn, at this pD (Figure 3e) the formation of $[(Fe(TPPS))_2O]^{8-}$ is nearly complete (proton frequencies (ppm): meta, 8.2; ortho, 7.5; pyrrole β, 13.7). This species is observed at lower pD (4.54, ~8 ppm); Figure 3b). The signals for $[(Fe(TPPS))_2O]^{8-}$ increase in intensity as the pD is increased (Figures 3b–g). Note the overlap of the $[(Fe(TPPS))_2O]^{8-}$ pyrrole β-proton signal at 13.7 ppm and the $[Fe(TPPS)(H_2O)_2]^{3-}$ ortho proton signal at 14.6 ppm in Figure 4c (pD = 5.60). With an increase in pD to 5.95, the intensity of the signal at 14.6 $[(Fe(TPPS)(H_2O)_2]^{3-}$, ortho proton) decreases and appears as a shoulder to the pyrrole β signal for $[(Fe(TPPS))_2O]^{8-}$ (Figure 3d). The limiting spectrum for $[(Fe(TPPS))_2O]^{8-}$ (Figure 3g) at pD 12.14 shows a split meta proton signal. There are no significant shifts in the signals for the individual species as the pD changes. Thus, all species for this system are in slow exchange.

$[Fe(TMPyP)]^{5+}$ NMR. The NMR spectra of $[Fe(TMPyP)]^{5+}$ between pD = 2.2 and pD = 12.3 are illustrated in Figures 5 (5.4–15.5 ppm) and 6 (48.0–78.0 ppm). The limiting spectrum for $[Fe(TMPyP)(H_2O)_2]^{5+}$ (pD = 2.19) is illustrated in Figures 5a and 6a (proton frequencies (ppm): methyl, 6.0; meta, 11.3; ortho, 14.4; pyrrole β, 70.5). At pD = 3.85, the same signals are reduced in intensity; these signals continue to decrease in intensity, broaden, and shift as the pD is increased (Figures 5b–j and 6b–e).

Table V. ^1H Chemical Shifts[a]

	pyrrole β	ortho	meta	methyl
$[Fe(TPPS)(H_2O)_2]^{3-}$	52.4	14.6	10.6	*c*
$[Fe(TPPS)(H_2O)(OH)]^{4-}$	33.4	*b*	*b*	*c*
$[(Fe(TPPS))_2O]^{8-}$	13.7	7.5	8.2/8.4	*c*
$[Fe(TMPyP)(H_2O)_2]^{5+}$	70.5	14.2	11.3	6.0
$Fe(TMPyP)(H_2O)(OH)]^{4+}$	*b*	*b*	10.5	5.7
$[(Fe(TMPyP))_2O]^{8+}$	14.4	8.4	9.6/9.2	*b*
$[Fe(TMPyP)(OH)_2]^{3+}$	62.0	*b*	9.3	*b*

[a] Chemical shift relative to DSS (ppm). [b] Unassigned. [c] Not applicable.

This behavior is assigned to the presence of $[Fe(TMPyP)(H_2O)(OH)]^{4+}$ as suggested previously for this system.[8] Thus, the axial ligand protons of the two monomeric forms are in fast exchange. The pH dependence of these proton signals display a profile appropriate for a diaquo–aquo/hydroxo equilibrium (vide infra). The signals for these monomeric species are not observed above a pD of 11.79 (Figure 5k,l). Figure 5d shows the presence of four new signals assigned to $[(Fe(TMPyP))_2O]^{8+}$ (proton frequencies (ppm): pyrrole β, 14.4; meta, 9.6, 9.2; ortho, 8.4 (the methyl proton signal is obscured by the water signal)). As the pD is increased to 7.04, there is an increase in intensity of these signals (Figure 5d–g), the intensity remains fairly constant between pD = 7.04 and pD = 8.59 (Figures 5g–h), and from pD = 8.59 to pD = 12.23, the signals decrease (Figures 5h–l) with no significant chemical shifts. A fourth species begins to appear by pD = 10.69 (Figure 5i) and is assigned to $[Fe(TMPyP)(OH)_2]^{3+}$ (proton frequencies (ppm): meta, 9.3; pyrrole β, 62.0 (Figure 6g,h)). These signals increase in intensity as the pD is increased (Figures 5i–l) and 6g,h) while the signals for the dimer decrease. Again, there are no significant chemical shifts for $[Fe(TMPyP)(OH)_2]^{3+}$ as the pD is increased. Chemical shift values for the various species are summarized in Table V.

Discussion

The axial ligation of water and water-derived ligands with the iron(III) atom in these water-soluble porphyrinate systems are clearly pH-dependent. We first consider the nature of the binuclear complex in the solid state. The other pH-dependent solution species for both the cationic and anionic porphyrinates are also addressed, along with the chemical equilibria involved.

A number of possible structures, other than the well-known μ-oxo-bridged complex with two five-coordinate iron(III) atoms, have been proposed for the oligomeric species formed by water-soluble iron(III) porphyrinates.[10,13,16,37-40] Suggested structures

(36) Landrum, J. T.; Hatano, K.; Scheidt, W. R.; Reed, C. A. *J. Am. Chem. Soc.* **1980**, *102*, 6729.

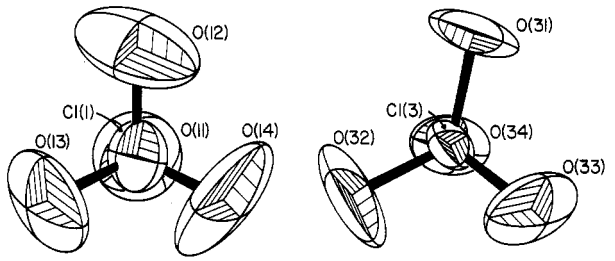

Figure 7. ORTEP2 drawing of "ordered" perchlorate anions (24% probability surfaces).

have included six-coordinate oxo-bridged iron(III) with water[16] or hydroxide ion[10,37] as the sixth ligand. Another suggested structure has water molecule(s) hydrogen bonded to the μ-oxo bridge,[38] a structural feature actually observed in the solid-state structure of $[Fe(FF)]_2O\cdot H_2O$.[39] Finally, a binuclear complex with a dihydroxy bridge has been suggested.[13,40] Our crystallographic and NMR studies clearly show that the high-pH binuclear $[Fe(TMPyP)]^{5+}$ complex is a five-coordinate μ-oxo species in the solid state and in solution. The structural features of the complex are well within the range of values found for μ-oxo species formed by analogous organic-soluble derivatives.[39,41-45] The average $Fe-N_p$ distance, the axial Fe–O bond distance, the iron out-of-plane displacement, and the intramolecular ring–ring separation for all μ-oxo complexes are recorded in Table IV. It is seen that $[(Fe(TMPyP))_2O]^{8+}$ has structural parameters that differ little from the several organic-soluble binuclear antiferromagnetically coupled high-spin iron(III) species. A possible exception is the $[Fe(FF)]_2O\text{-}H_2O$ species,[39] where the covalently attached porphyrin halves may affect the coordination parameters. Thus the structural data for $[(Fe(TMPyP))_2O]^{8+}$ clearly show that its aqueous environment has not led to any unusual coordination features.

Our structural results for the water-soluble iron derivatives lead us to speculate on the general difficulties of obtaining crystal structures for this class of compound. Only two crystal structure determinations for water-soluble metalloporphyrin derivatives have been previously reported.[25,46] We have had relatively limited success in obtaining crystals for these iron complexes despite trying a wide variety of experimental conditions. Moreover, the crystalline $[(Fe(TMPyP))_2O]^{8+}$ derivative that was obtained appears to suffer from severe crystallographic problems that have no ready solution. Difficulties in obtaining crystals result from the fact that there are a limited number of counterions that yield salts with appropriate solubilities. For the positively charged water-soluble derivatives, apparently the best counterion is the perchlorate ion. However, the perchlorate anion has well-known disorder problems, and indeed two of the four unique perchlorate ions in $[(Fe(TMPyP))_2O]^{8+}$ are seriously disordered. Moreover, even the "ordered" perchlorate ions have substantial thermal motion that must result from excessive positional freedom in their lattice cavities.

The large thermal motion of these "ordered" anions is illustrated in Figure 7. The thermal motion of the oxygen atoms appears to be much larger than expected, especially perpendicular to the Cl–O bond. Indeed, a calculation of the oxygen atom root-mean-square-displacements (RMSD) and the direction each component makes with respect to the Cl–O bond confirms this. These values are tabulated in Table SV. For each oxygen atom, the intermediate and maximum RMSD's are 2–4 times larger than the minimum RMSD. The minimum RMSD component for each oxygen atom is approximately along the bond axis while the other principal components are approximately perpendicular to the bond direction. The overall appearance suggests substantial rotational freedom in each lattice perchlorate cavity. Consistent with the idea that the perchlorates are not particularly constrained in the lattice, typically only one or two oxygen atoms of each perchlorate ion have short interatomic contacts with porphyrin atoms (the peripheral methylpyridinium-4-yl groups). The geometry of these oxygen···methylpyridinium-4-yl interactions in the lattice are consistent with ion pairs as observed in *N*-methylpyridinium iodide.[47] The remaining oxygen atoms have much longer interatomic distances (>3.2 Å). This apparently poor packing of the perchlorate ions is found even though the experimental densities of three crystalline water-soluble metalloporphyrin derivatives (1.57 g/cm^3 for $[Fe(TMPyP)]_2O(ClO_4)_8\cdot 4H_2O$, 1.62 g/cm^3 for $[Fe(TMPyP)](H_2O)_2(ClO_4)_5$, 1.47 g/cm^3 for $[Ni(TMPyP)](HIm)_2(ClO_4)_4\cdot 2C_3H_6O$,[25] and 1.63 g/cm^3 for $Co(TAPP)(HIm)_2I_5\cdot 5H_2O$[46] (calculated)) are normal by comparison to those of analogous H_2TPP derivatives. Anions with substantially more hydrophobic character than perchlorate and yet appropriate solubilities would appear to be the ideal anions required to obtain improved crystals.

Scheme I

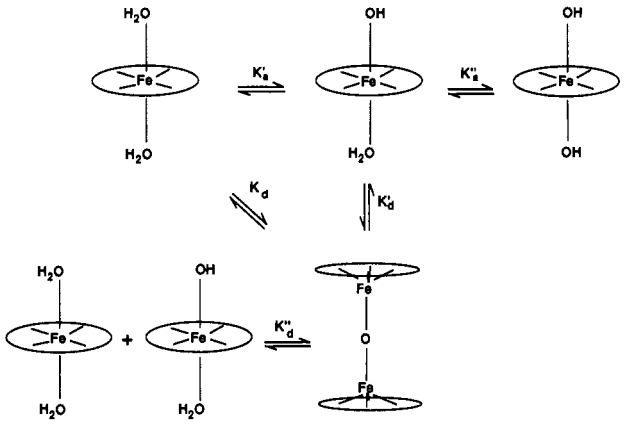

The NMR splitting pattern of the meta protons of the peripheral phenyl groups of tetraarylmetalloporphyrins can be used to deduce the position of the metal atom with respect to the porphyrin plane.[48] When the metal atom is six-coordinate, it is generally expected to be in the porphyrin plane and yield one meta proton signal. Five-coordinate iron(III) is expected to be significantly out-of-plane and to give split meta proton signals. The spectra of the monomeric species for both $[Fe(TPPS)]^{3-}$ and $[Fe(TMPyP)]^{5+}$ systems show six-coordinate characteristics while the binuclear μ-oxo species are five-coordinate. Scheme I illustrates the probable solution species as a function of pH and the most likely position of the iron(III) atom with respect to the porphinato core for each complex. Also the spin state of the iron(III) can be assigned from the pyrrole β-proton signals.[49] In high-spin or nearly high-spin iron(III) tetrarylporphyrin derivatives, these signals occur from 60 to 80 ppm. Formation of quantum-admixed intermediate-spin ($S = {}^5/_2, {}^3/_2$) iron(III) leads to shifts >20 ppm;[50] a precise boundary of pyrrole β-proton chemical shifts for pure high-spin and admixed intermediate-spin systems does not appear to be well-defined. The formation of a

(37) Kolski, G. B.; Plane, R. A. *J. Am. Chem. Soc.* **1971**, *94*, 3740.
(38) Miller, J. R.; Taies, J. A.; Silver, J. *Inorg. Chim. Acta* **1987**, *138*, 205.
(39) Landrum, J. T.; Grimmett, D.; Haller, K. J.; Scheidt, W. R.; Reed, C. A. *J. Am. Chem. Soc.* **1981**, *103*, 2640.
(40) Goff, H.; Morgan, L. O. *Inorg. Chem.* **1976**, *15*, 2062.
(41) Lay, K. L.; Buchler, J. W.; Kenny, J. E.; Scheidt, W. R. *Inorg. Chim. Acta* **1986**, *123*, 91.
(42) Hoffman, A. B.; Collins, D. M.; Day, V. W.; Fleischer, E. B.; Srivastava, R. S.; Hoard, J. L. *J. Am. Chem. Soc.* **1972**, *94*, 3620.
(43) Swepston, P. N.; Ibers, J. A. *Acta Crystallogr., Sect. C* **1985**, *C41*, 671.
(44) Radonovich, L. J.; Caughey, W. S.; Hoard, J. L. Unpublished results.
(45) Bartczak, T. J.; Latos-Grazynski, L.; Wyslouch, A. *Inorg. Chim. Acta* **1990**, *171*, 205.
(46) Guangdi, Y.; Xizhang, C.; Fengshan, W.; Guodong, Z. *Jilin Univ. Nat. Sci. Soc.* **1988**, *3*, 118.
(47) Lalancette, R. A.; Furey, W.; Costanzo, J. N.; Hemmes, P. R.; Jordan, F. *Acta Crystallogr., Sect. B* **1978**, *B34*, 2950.
(48) La Mar, G. N.; Walker, F. A. In *The Porphyrins*; Dolphin, D., Ed.; Academic: New York, 1978; Vol. 4, pp 79–81.
(49) Goff, H. M. In *Iron Porphyrins*; Gray, H. B., Lever, A. B. P., Eds.; Addison-Wesley: Reading, MA, 1986; Vol. 1, pp 237–283.
(50) Boersma, A. D.; Goff, H. *Inorg. Chem.* **1982**, *21*, 581.

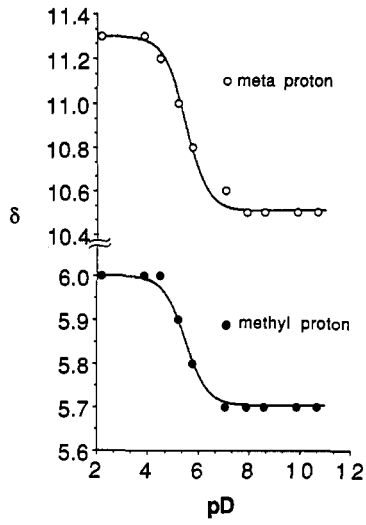

Figure 8. Plot of the chemical shifts of the meta and methyl protons of $[Fe(TMPyP)(H_2O)_2]^{5+}$ vs pD. Solid line shows calculated values for a $pK'_a = 5.5$ process.

μ-oxo binuclear complex with its antiferromagnetically coupled high-spin iron(III) atoms leads to pyrrole β-proton signals at approximately 13–14 ppm.[49] We thus expect that the pH dependent pyrrole β-proton and meta proton NMR signals can be used to deduce the likely solution species for the water-soluble iron porphyrinates. Both sets of the pH-dependent NMR data provide direct evidence for distinct axially ligated species. At low pH, both water-soluble ferric porphyrinate systems form monomeric diaquo species. Increasing the pH leads to loss of proton(s) and the formation of a mixed axial ligand complex, followed by the formation of a binuclear species and finally, at higher pH still, re-formation of a monomeric complex.

The $[Fe(TMPyP)]^{5+}$ system is more complicated than the $[Fe(TPPS)]^{3-}$ system. At pD = 2.19 (Figure 5a), a single meta proton signal at 11.3 ppm and a pyrrole β-proton signal at 70.5 ppm are found as expected for six-coordinate $[Fe(TMPyP)(H_2O)_2]^{5+}$. Other signals are from the *N*-methyl protons at 6.0 ppm and the ortho protons at 14.2 ppm.[51] The spectrum remains constant until pD = 3.85 where three new signals are observed and are assigned as the phenyl meta (9.2 and 9.6 ppm) and ortho (8.4 ppm) protons of $[(Fe(TMPyP))_2O]^{8+}$.[21] As expected, these signals increase in intensity as the concentration of the μ-oxo complex increases with increasing pD (Figure 5b–g). In the intermediate pD region, no discretely observed signals that could be assigned to the mixed-ligand aquo/hydroxo species were found. However, all four proton signals assigned to the diaquo complex display both broadening and shifting with increasing pD consistent with an exchange process involving a new species (aquo/hydroxo, vide infra). At higher pD, commencing at 10.69, signals at 9.3 ppm and, at pD = 11.39, 62 ppm are observed. We assign these signals to the formation of a new monomeric species, the dihydroxy complex $[Fe(TMPyP)(OH)_2]^{3+}$ (Scheme I). At pD = 12.23 (the highest practicably obtainable), these signals account for about 75% of the total signal observed. The formation of the dihydroxy complex $[Fe(TMPyP)(OH)_2]^{3+}$ would be expected to occur at lower pD than that of the $[Fe(TPPS)(OH)_2]^{5-}$ complex owing to the overall positive charge on the tetrakis(*N*-methylpyridinium-4-yl)porphyrin species.

The meta proton peak of the diaquo complex is observed to shift as a function of increasing pD. This behavior is consistent with a proton-dependent process, most probably K'_a of Scheme I. At low pD, this peak is found at 11.3 ppm but the peak shifts upfield as the pD is increased and becomes constant at 10.5 ppm at pD = 8–10. A plot of the chemical shift as a function of pD allows calculation of the apparent pK_a of the process (see Figure 8). The value obtained from the plot of chemical shift vs pD, 5.5, is in good agreement with the pK'_a values obtained by other workers for this process.[52] Hence, the NMR data are interpreted as providing strong indirect evidence for the mixed aquo/hydroxo complex $[Fe(TMPyP)(H_2O)(OH)]^{4+}$. A similar chemical shift/pH profile is observed for the methyl proton peak although the total variation in shift is only 0.3 ppm. The apparent pK_a for this set of shifts is also 5.5. Both sets of chemical shift data are plotted in Figure 8 as well as calculated curves for a $pK'_a = 5.5$ process. The other coexisting species in this pD range is, of course, the μ-oxo complex $[Fe(TMPyP))_2O]^{8+}$. We also observe, as did Miskelly et al.,[8] the expected reduction (Scheme I) in the proportion of the μ-oxo binuclear complex upon reduction of the total porphyrin concentration at a given pH.

Finally, the ^1H NMR spectrum of crystalline $[(Fe(TMPyP))_2O](ClO_4)_8 \cdot 4H_2O$ (6.0×10^{-3} M in DMSO-d_6) gave a spectrum[53] that is virtually identical with the predominant spectrum in aqueous solution at intermediate pD (Figure 5d–h). These similar NMR shifts establish a link to the structural definition of the complex and clearly identify the formation of $[(Fe(TMPyP))_2O]^{8+}$ at intermediate pD.

The NMR spectrum of the $[Fe(TPPS)]^{3-}$ system at pD = 2.3 (Figure 3a) shows a single meta proton signal at 10.6 ppm and a pyrrole β-proton signal at 52.4 ppm (Figure 4a). These two spectral characteristics are clearly consistent with the assignment of this species as $[Fe(TPPS)(H_2O)_2]^{3-}$. The other observed resonance (14.6 ppm, Figure 3a) can be assigned to the ortho proton of this species. The NMR spectra are unchanged as the pD is increased, until at pD = 4.94, a second pyrrole β-proton signal appears at 33.4 ppm while the original signal at 52.4 ppm remains (Figure 4b). The original meta proton signal at 10.6 ppm remains a singlet, but a new broad signal at 8 ppm appears. The intensity of the ~8 ppm signal increases and is resolved into two separate lines that become increasingly distinct and intense as the pD is increased (Figure 3b–f). These signals are clearly the meta and ortho protons of $[(Fe(TPPS))_2O]^{8-}$ whose concentration is increasing. Concomitantly, the intensity of the meta and ortho protons of $[Fe(TPPS)(H_2O)_2]^{3-}$ decrease. In the intermediate pD region, the 14.6 ppm ortho proton signal of the diaquo complex and the 13.7 ppm pyrrole β signal of μ-oxo are seen to overlap. The limiting high pD spectrum (11.74) is that of $[(Fe(TPPS))_2O]^{8-}$. The meta proton signal is split into two peaks as expected for five-coordinate iron(III). We believe that the small signal at 33.4 ppm is to be assigned to the pyrrole β-protons of the singly deprotonated species ($[Fe(TPPS)(H_2O)(OH)]^{4-}$). The upfield shift of this pyrrole β signal relative to that of diaquo (52.4 ppm) is consistent with the mixed ligand aquo/hydroxo complex having a lower magnetic moment than the diaquo complex and is compatible with the weaker ligand field of hydroxide ion. As would be expected (Scheme I), this 33.4 ppm signal disappears at higher pD (above ~5.6) along with the signal at 52.4 ppm, and at pD = 7.04 (Figure 3e), the formation of the binuclear complex is nearly complete.

Two differences in the $[Fe(TPPS)]^{3-}$ and $[Fe(TMPyP)]^{5+}$ systems are notable and require explanation. First, why is the aquo/hydroxo mixed ligand intermediate seen as a discrete species only for the $[Fe(TPPS)]^{3-}$ system and not in the $[Fe(TMPyP)]^{5+}$ system? Second, why are the pyrrole β-proton signals for the low pH forms seen at different positions? The exchange of the protons in the $[Fe(TPPS)]^{3-}$ system at low to intermediate pH is found to be catalyzed by a general-acid/general-base process. Consistent with this, the 52.4 and 33.4 ppm pyrrole β-proton signals are both broadened upon addition of acetate buffer at constant ionic strength in the pH range where both signals are observed. In the absence of added buffer, general acid/base catalysis is enhanced by the ~2 pH unit difference in the pK_a values ($pK_a \approx 6.7$ for $[Fe(TPPS)]^{3-}$ and 5.4[8] for $[Fe(TMPyP)]^{5+}$). The concentration

(51) Goodwin, J.; Scheidt, W. R. *J. Phys. Chem.* **1990**, *94*, 4432. The proton signals reported for $[Fe(TMPyP)(DMSO)_2]^{5+}$ occur at similar chemical shifts to those we have observed for $[Fe(TMPyP)(H_2O)_2]^{5+}$.

(52) The range of previously reported values for this pK'_a range from 5.3 to 5.8. See Table VI of Miskelly et al.[8]

(53) Proton frequencies relative to TMS (ppm): pyrrole β, 14.3; meta, 9.7, 9.5; ortho, 8.4; methyl, 4.8.

Table VI. Dimerization and Acid Dissociation Constants[a] for the (Tetrakis(sulfonatophenyl)porphyrin)iron(III) System

pK'_a	log K_d	log K'_d	log K''_d	μ, M	temp, °C	ref
	−8.1			0.1	25	16
	−6.5			1.0	25	16
8.1				1.0	23	18
8.1				0.1	25	14
	−6.4			0.1	35	13
	−8.6				20	17
7.0 ± 0.2	−8.3	5.9	−1.1	0.1	25	19
6.5 ± 0.2	−7.3			0.3	25	19
6.7	−9.6	3.8	−2.9	0.1	25	this work
	−9.0			0.2	25	this work

[a] Equilibrium constants defined in Scheme I.

effects of added buffer on the broadening of the $[Fe(TPPS)]^{3-}$ signals are compatible with this. More rapid proton exchange may also be enhanced by better peripheral charge neutralization in the $[Fe(TMPyP)]^{5+}$ system. The differences in the positions of the pyrrole β-proton signals in the two diaquo complexes probably reflect small differences in spin state. Strouse and co-workers[54] have shown that effects such as the number of hydrogen bonds formed by the axial aquo ligands have a measurable effect on the bulk magnetic susceptibility of $[Fe(TPP)(H_2O)_2]ClO_4$ derivatives.

Values of the equilibrium constants for dimer formation K_d, K'_d, and K''_d (see Scheme I) and the deprotonation of the diaquo complex, K'_a, for $[Fe(TPPS)]^{3-}$ can be obtained from concentrations estimated from integrations of the NMR signals. Our estimates along with previously reported values are tabulated in Table VI. The dimer formation constant of μ-oxo from the diaquo complex, K_d, was obtained by integrating the meta proton signals for $[Fe(TPPS)(H_2O)_2]^{3-}$ and $[(Fe(TPPS))_2O]^{8-}$ at specific pD's. The values of log K_d (−9.6 (μ = 0.1) and −9.0 (μ = 0.2)) follow the same ionic strength dependence seen previously.[19] Our estimate for pK'_a, where $K'_a = [Fe(TPPS)(H_2O)(OH)]^{4-}[H^+]/[Fe(TPPS)(H_2O)_2]^{3-}$, was made by estimating concentrations from the integration of the pyrrole β-protons. This estimate is significantly lower than the values previously obtained (see Table VI); the differences are attributed to the fact that the pK'_a is determined by integrating these very broad signals. K''_d was calculated from K_d and K'_a where log $K''_d = -2.9$. K'_d was estimated from the same values where log K'_d = log $(K_d/(K'_a)^2)$ = 3.8. The comparison of our values, obtained by NMR integrations, with those obtained earlier (Table VI) are consistent with correct NMR assignments.

In summary, the nature of the pH-dependent axial ligands with ferric water-soluble porphyrins have been determined from the pH-dependent proton NMR spectra. Four distinct species have been found for the $[Fe(TMPyP)]^{5+}$ system and three for the $[Fe(TPPS)]^{3-}$ system. The μ-oxo complex of $[Fe(TMPyP)]^{5+}$ is found to be a five-coordinate binuclear complex in the solid state with a structure similar to those of organic-soluble (μ-oxo)ferric porphyrinate species.

Acknowledgment. We thank the National Institutes of Health for the financial support under Grant GM-38401, Drs. F. A. Walker, J. Goodwin, and S. Mitra for helpful discussions concerning the NMR studies, Dr. B. Finzel for his suggestions concerning solvent disorder, and Prof. C. E. Strouse for a copy of C. M. Ceccio's thesis.

Supplementary Material Available: Table SI (complete crystallographic details), Table SII (anisotropic thermal parameters), Table SIII (rigid group parameters of one perchlorate anion and one *N*-methylpyridinium-4-yl ring), Table SIV (crystallographic coordinates for the rigid group atoms for the *N*-methylpyridinium-4-yl ring and perchlorate anion), Table SV (angles between major, intermediate, and minor axes of the oxygen RMSD's along the Cl–O bonds of the perchlorate ions), Table SVI (complete bond distances and angles), and Table SVII (mean plane calculations) (14 pages); a listing of observed and calculated structure amplitude data (×10) (21 pages). Ordering information is given on any current masthead page.

(54) Ceccio, C. M. Masters Thesis, University of California, Los Angeles, 1988. Strouse, C. E. Personal communication.